Wax crystallization and aggregation in a model crude oil

2005 J. Phys.: Condens. Matter 17 S3651

(http://iopscience.iop.org/0953-8984/17/45/061)

INSTITUTE OF PHYSICS PUBLISHING JOURNAL OF PHYSICS: CONDENSED MATTER

J. Phys.: Condens. Matter **17** (2005) S3651–S3660 doi:10.1088/0953-8984/17/45/061

Wax crystallization and aggregation in a model crude oil

Emanuele Vignati[1,4], Roberto Piazza[1], Ruben F G Visintin[2,4], Romano Lapasin[2], Paolo D'Antona[3,5] and Thomas P Lockhart[3]

[1] CSGI-Politecnico Milano, piazza Leonardo da Vinci, Milano (MI), Italy
[2] DICAMP, Università di Trieste, piazzale Europa 1, 34127 Trieste (TS), Italy
[3] EniTecnologie SpA, Via Maritano 26, 20097 San Donato Milanese (MI), Italy

Received 3 October 2005
Published 28 October 2005
Online at stacks.iop.org/JPhysCM/17/S3651

Abstract

The high-molecular-weight paraffinic ('wax') fraction separates from crude oils at low temperatures, a process that can lead to a sol–gel transition when the mass of wax solids exceeds 1–2%. Attractive interactions between the micron-size wax solids suspended in the non-polar medium have been suggested to be responsible for gel formation. The present study reports an optically transparent model oil system, based on a mixture of linear and branched paraffins. Rheological measurements and optical microscopy show that the model system reproduces essential features of crude oil gels. Small-angle light scattering studies conducted at temperatures intermediate between the cloud point (58 °C) and sol–gel transition (39 °C) show that phase separation and wax solid aggregation are rapid processes, leading to the formation of dynamically arrested structures well above the sol–gel transition determined rheologically. Analysis of gravity settling effects has provided a rough estimate for the yield stress of the wax particle network formed (greater than 0.7 Pa at 45 °C and 0.07 Pa at 55 °C). Clusters formed by the aggregated wax solids possess a fractal dimension of about 1.8, consistent with diffusion-limited cluster–cluster aggregation.

1. Introduction

The paraffinic (wax) component of crude oils is prone to phase separation (crystallization) at low temperature. The temperature at which wax crystals first appear as an oil is cooled is defined as the *cloud point* (CP), or the wax appearance temperature. Wax deposits can form on the walls of pipelines where the temperature of the external environment is below the CP, a situation commonly encountered in offshore and arctic production (Singh *et al* 2000). Because wax

[4] Current address: EniTecnologie SpA, Via Maritano 26, 20097 San Donato Milanese (MI), Italy.
[5] Current address: Eni E&P divisione: via Emilia 1, 20097 San Donato Milanese (MI), Italy.

deposition leads to progressive restriction of the pipeline, oil companies invest considerable effort into evaluating the risk of deposit formation and defining effective countermeasures.

Below the CP, many crude oils undergo a rheological transition over a narrow temperature range to a gel-like phase characterized by a significant yield stress. This is referred to as the *pour point* (PP), which, as the name suggests, corresponds to the temperature below which, in a standard test, the crude oil no longer flows. Crude oil gelation represents a threat wherever the temperature external to the pipeline lies below the PP of the oil: prolonged interruption of flow will lead to cooling of the oil and, inevitably, gelation. Because the gelled oil displays yield behaviour, significant pressure must be applied to re-start flow; in many operational scenarios, the pipeline may not be able to withstand this pressure. Thus, predicting the conditions for oil gelation and the pressure required to re-start flow are also important in the design of offshore/artic field developments (Chang *et al* 1999).

Crude oil gelation is associated with phase separation of the wax component, and may take place when as little as 1–2% of wax solids have formed (Rønningsen and Bjorndal 1991, Kané *et al* 2003). Chemical studies have shown that wax deposits from crude oils contain both higher-weight linear and branched alkanes (Rønningsen and Bjorndal 1991). The complexity of and wide variation in the composition of crude oils generates a very wide range in CP and PP behaviours. For most crude oils the CP falls between 20 and 60 °C. The PP may lie from 10 to 50 °C below the CP and, for some crude oils, no PP is found over the range of operational interest.

The oil gelation process has captured the interest of workers in the field at least since the first decades of the past century (cf Padgett *et al* 1926). Recently, we have formulated a colloidal gel hypothesis to account for the PP behaviour of crude oils, invoking attractive interactions between the small wax solids which lead to network formation (Visintin *et al* 2005). This hypothesis is supported by optical microscopy and rheological results, and accounts for many properties of the gels, including their ability to re-heal partially following shearing. From the point of view of colloid science, a distinctive aspect of the gelation process is the competition between paraffin crystal growth and the aggregation of the single wax crystallites into a dynamically arrested structure. That is, unlike other well studied gel forming colloidal systems, here the associating particles are not present in the fluid initially, but rather form and increase in size at a rate which is fixed by crystal nucleation and growth, a physical mechanism which is totally distinct from the diffusion-limited gelation of the system.

Unfortunately, more direct studies to further elucidate the gelation process and network characteristics, such as might be achieved through the application of optical methods, are impeded by the strong absorption of crude oils in the UV and visible range, and by their fluorescence. In the present contribution, a model system is reported which is colourless and transparent and is amenable to light scattering investigations at temperatures intermediate between the CP and the PP. The model system duplicates several key characteristics of crude oil gels, and is employed to verify and further probe the processes involved in the formation of wax crystal aggregates.

2. Materials and methods

2.1. Sample preparation and handling

The conditioning treatment for the sample prior to rheological testing involved heating to 60 °C for 1 h while stirring in a beaker. Samples used in the light scattering experiments were instead heated directly in the measurement cell to 80 °C. Observation under optical microscopy indicated that no wax solids existed after heating above 60 °C, and experimental results showed good repeatability.

2.2. Rheological studies

Rheological measurements were carried out using controlled stress (DSR200 by Rheometric Scientific and RS 150 by Haake) and controlled strain rheometers (RFSIII by Rheometric Scientific) equipped with different geometries (helical, vane, couette, cone and plate and parallel plate) depending on the temperature and viscosity of the sample. The rheometer, whose temperature was controlled by a thermal bath, was statically cooled from the starting temperature (typically 50 °C) to the final (holding) temperature at a programmed cooling rate. More details on the cooling programs and the testing procedures are reported elsewhere (Visintin *et al* 2005). Both steady-state and oscillatory measurements were carried out. Steady-state measurements were conducted in order to evaluate the viscosity and yield stress from the flow curve profile (viscosity versus stress). In the controlled stress test, each shear stress was applied long enough to reach the stationary state at each testing temperature. Oscillatory measurements at small amplitude were carried out in order to obtain information on the kinetics of gel formation as a function of temperature and on the strength of the gel formed.

2.3. Small-angle light scattering

For the small-angle light scattering (SALS) studies the output from a 17.5 mW fibre-coupled laser diode (wavelength, 658 nm) was collimated to a beam waist $w \approx 1.3$ mm and fed through the cell. Owing to the strong scattering power of the system investigated, the optical path had to be kept as short as possible, compatible with the manipulation of the viscous fluid and the ability to maintain accurate control of the sample temperature. To fulfil these requirements, a custom-made flow-through cell (Hellma, Germany), was used. This consisted of a 5 mm thick rectangular quartz frame into which a cylindrical sample chamber (diameter 8 mm, optical path 200 μm) had been bored, together with inlet/outlet channels designed to ensure efficient and homogeneous filling. The quartz frame was tightly enclosed in a copper box in thermal contact with a Peltier module, which provided temperature control to better than 0.1 K, and allowed temperature ramps at rates up to 5 °C s^{-1}. As is commonly done, the Fourier-transforming properties of a lens were exploited to obtain a 1–1 mapping of the scattered wavevectors on the focal plane of a large f-number achromatic doublet. An additional inverted telescope, placed between the cell and the Fourier lens, de-magnified the angular scattering pattern, allowing larger scattering angles to be reached. This set-up provided measurement over an angular range in air from $0.8° < \theta < 13°$ (corresponding to $0.35 < q < 15 \times 10^3$ cm^{-1}) imaged onto the detecting CCD sensor.

2.4. Materials

The normal (n)-paraffins employed were obtained from a commercial source, while the iso-paraffins were obtained by cracking of the n-paraffins. The molecular weight distributions of the two paraffins employed are reported in figure 1. The solvent employed was a blend of branched hydrocarbons with carbon numbers in the range C_{11}–C_{14} (Soltrol 130, Chevron Phillips Chemicals Italy).

3. Results and discussion

3.1. The model oil

The model oil employed in these studies consisted of a mixture of high-mw linear (C_{20}–C_{55}) and branched paraffins (C_{18}–C_{38}) dissolved in a saturated hydrocarbon solvent (C_{11}–C_{14}).

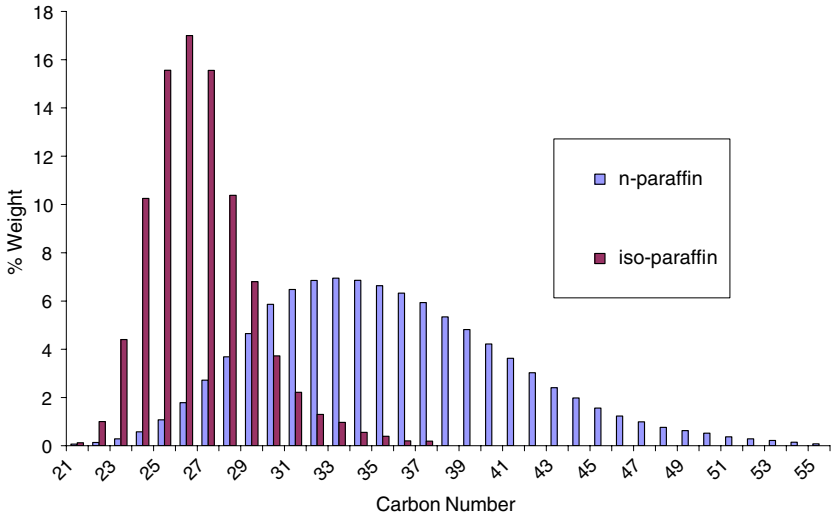

Figure 1. Composition of n- and iso-paraffins used in model system.

(This figure is in colour only in the electronic version)

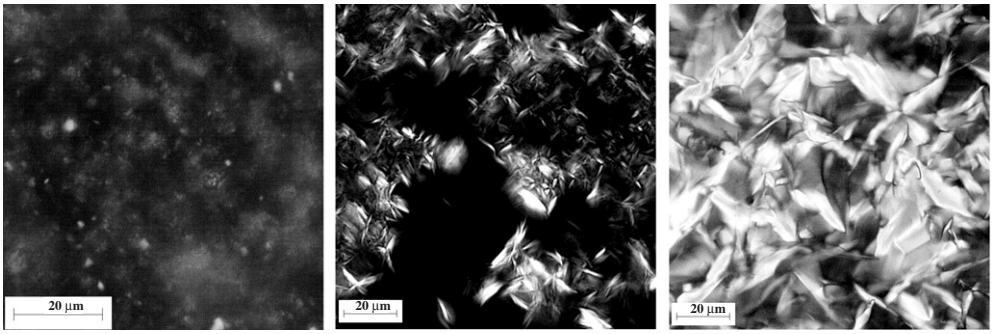

(a) (b) (c)

Figure 2. Polarized microscopy images of (a) a crude oil, (b) the model system and (c) the model with only n-paraffin waxes, all below their respective PP (the bar is 20 μm).

The concentration of the n- and iso-paraffins was adjusted to achieve wax crystallization and gelation over a temperature range convenient for the experimental studies (CP, 58 °C; PP, 39 °C). Addition of the branched paraffins proved essential to obtaining a system that closely mimics the gelation behaviour of real crude oils. Though this result is perhaps not surprising in light of Rønningsen's findings on the composition of the wax solids formed from real crude oils (Rønningsen and Bjorndal 1991), model systems reported in the literature have generally been composed of only linear paraffins dissolved in a low-molecular-weight solvent (see, for example, Kané *et al* 2003, Singh *et al* 2000, Holder and Winkler 1965). The effect of branched paraffins on crystal morphology is shown in figure 2, which compares the aggregated masses of sheet-like crystals present in a typical crude oil with those obtained for the model oil and for a solution containing only the linear high-molecular-weight paraffins dissolved in the solvent (all were cooled to below their respective PPs).

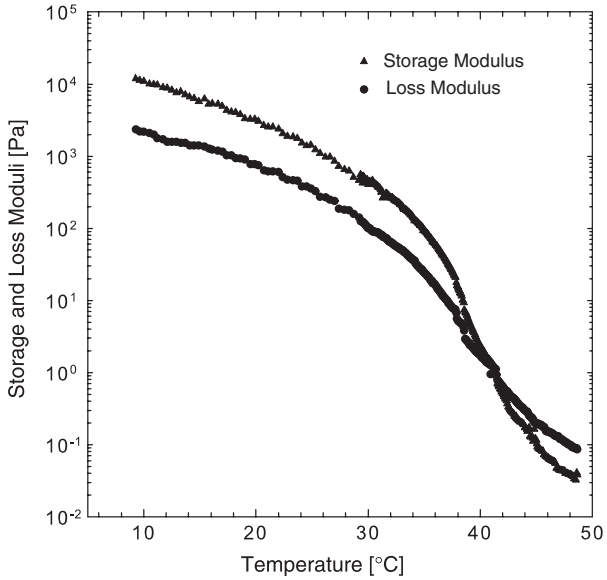

Figure 3. Storage and loss moduli versus temperature for the model system in cure tests at a fixed cooling rate (1 °C min^{-1}).

Inspection of the figure shows that, while much sharper images are obtained with the model system, the general characteristics resemble those of the crude oil: the solid phase appears to be composed of ill formed, sheet-like crystals amassed into clusters of about 10 μm size, which further aggregate to form a space-filling network. The crystals formed by the n-paraffins in the absence of the iso-component are much larger, suggesting that the branched paraffins interfere with the regular growth of the wax crystals. This is also evident in DSC experiments, in which the solution of linear paraffins displays a much sharper crystallization transition than either the crude oil or the model system including branched paraffins (results not shown).

The model closely resembles the crude oil in terms of its rheological behaviour. In particular, the storage and loss moduli (figure 3) and the shear viscosity (figure 4) increase several orders of magnitude over a relatively narrow temperature range around the PP.

Also, the ultimate gel strength is approached asymptotically over time at isothermal conditions below the PP and, most characteristically, the rheological properties of the colloidal gel formed are, to a large extent, recovered following shearing. In figure 5 we can see the time evolution of the storage modulus for model crude oil after different thermo-rheological histories. These results can be compared to analogous rheological measurements reported for a waxy crude oil (Visintin *et al* 2005).

3.2. Wax crystallization and aggregation

Rheological measurements are best interpreted with reference to the structural properties of the system. Optical microscopy provides a static image of the solids formed in the model oil when these have grown to a certain size, but open questions include whether the formation of a dynamically arrested, disordered structure takes place just at the PP, or whether it precedes the attainment of a finite shear modulus. Further, it is of interest to probe the competition between wax crystallization and crystallite aggregation, which suggest that the gel structure is kinetically determined; i.e., dependent on the cooling rate. One advantage of the model system

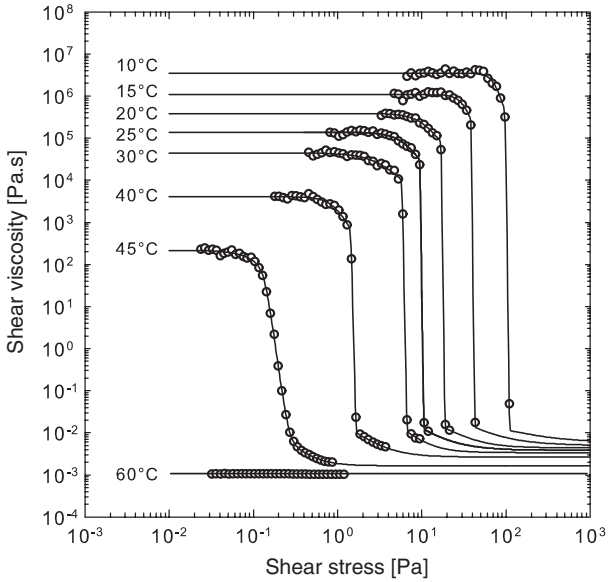

Figure 4. Flow curves at different temperatures for the model system. Continuous lines represent data fitting with the RBC model (Roberts *et al* 2001).

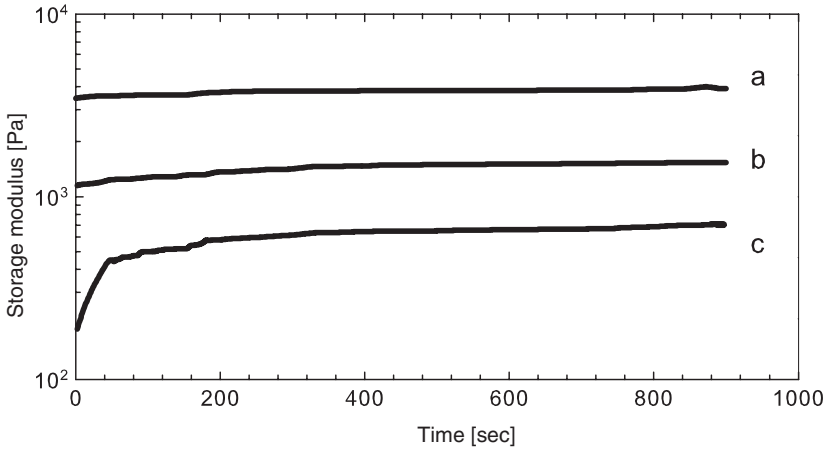

Figure 5. Time evolution of the storage modulus for the model system after the final temperature was reached. All samples were cooled to 20 °C at 1 °C min^{-1}: sample (a) was monitored in quiescent condition, sample (b) was sheared for 360 s at 0.01 s^{-1} after achieving the hold temperature and sample (c) was sheared at 1 s^{-1} for the time required to attain the final condition. The asymptotic value for the unperturbed case is higher than for the others: 3930 Pa for (a), 1536 Pa for (b) and 720 Pa for (c).

employed is that it permits, within certain limits, optical investigation of the solution structure below the CP. Thus, we have employed SALS to investigate the nature of the arrested phase and its dependence on the cooling rate.

In general terms, the temperature dependence of the optical properties of the model system can be described as follows: at high temperature the system is fully transparent, scattering as an ordinary fluid mixture. Below 60 °C the extinction coefficient α of the system increases

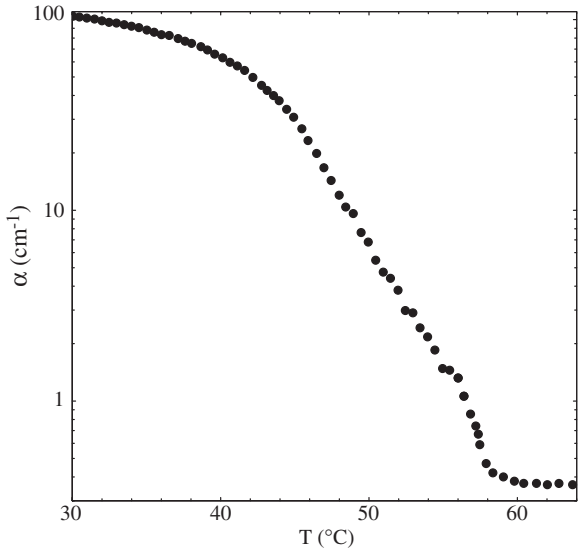

Figure 6. Temperature dependence of the extinction coefficient for the model system (cooling rate, 1 °C min^{-1}).

significantly, rapidly reaching large values (figure 6). The curve begins rounding off around 42 °C (i.e., close to the PP determined by rheological measurement), and for lower temperatures the total scattering cross section increases at a much lower rate. Although the extinction coefficient depends on the size of the scattering particles as well as on the total amount of solid phase, this trend suggests that most of the wax crystallization takes place within the temperature range where α shows the highest growing rate. The temperature dependence of the extinction coefficient does not show appreciable changes if the cooling is varied between 0.05 and 2 °C min^{-1}. Finally, we point out that an appreciable contribution to the scattering intensity comes from depolarized scattering, indicating the presence of optically anisotropic scatterers, which we identify as the wax crystallites. Polarized microscopy observations on the sample, performed at 30 °C after cooling from the fluid state at 2 °C min^{-1}, confirm the strong optical anisotropy of the wax particles.

Owing to the strong sample opalescence in the presence of wax solids, light scattering measurements close to the PP are precluded, even with the short optical cell employed in this study. Attempts to index-match the mixture by progressively adding another solvent (m-cresol) failed to reduce the extinction factor sufficiently. Therefore, SALS measurements were limited to temperatures greater than 48 °C, corresponding to a minimum transmission of about 80%, so that multiple-scattering effects are rather weak. Samples were first homogenized by heating the cell at 80 °C for 30 min, and then driven to the final temperature at a cooling rate of 1 °C min^{-1}.

An interesting question concerns the structure of the suspension between the CP and PP where, although the system appears 'macroscopically' fluid (that is, it flows under negligible mechanical stress), and rheological measurements show that the loss modulus is larger than the storage modulus, an appreciable amount of dispersed solid phase is already present. A first observation is that the small-angle speckle pattern detected by the CCD camera becomes completely frozen just below the CP. This means that the system is fully dynamically arrested (i.e., the system is fully non-ergodic, denoting the absence of particle motion or rearrangement).

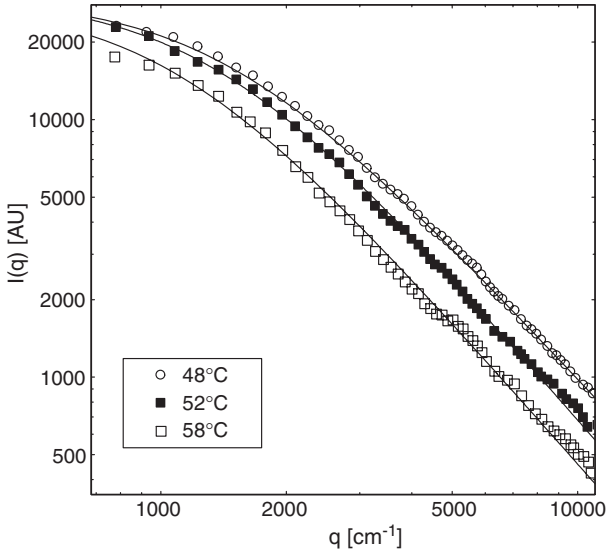

Figure 7. Small-angle scattering pattern for the model system at different temperature. Full lines are fits according to equation (1).

Therefore, although the storage modulus at these temperatures is very low (see figure 3), the system possesses many properties typical of a physical gel. Very small perturbations, however, cause weak zones to collapse internally, preventing fully developed gel behaviour.

SALS results obtained at three different temperatures are plotted in figure 7, in which a pronounced increase of the intensity scattered is found at small angles below 60 °C. A quantitative discussion of the scattering profiles requires some preliminary considerations. Usually, the intensity of the light scattered by a structured colloidal fluid is written as $I(q) = cP(q)S(q)$, where c is the particle concentration, $P(q)$ is the form factor for a single particle ('monomer') and $S(q)$ is the suspension structure factor. However, such a factorization is useful only where the monomer form factor has been determined independently, for instance from measurements on very diluted suspensions. This certainly does not apply to the situation we are considering, where the 'monomer' size and morphology may vary depending on the specific aggregation conditions. Nonetheless, provided that the wax crystallites are not so large as to show a strongly forward-peaked scattering profile, the form factor contribution to the intensity scattered can be neglected at sufficiently small q-vectors. This approach is comforted by the observation, for $T > 50\,^{\circ}\mathrm{C}$ and $q < 10^4\ \mathrm{cm}^{-1}$, that all scattering profiles are fitted reasonably well by the Fisher–Burford expression for the structure factor of a fractal colloidal gel:

$$S(q) = \frac{S_0}{\left[1 + \frac{2}{3d_\mathrm{f}}(qR_\mathrm{g})^2\right]^{d_\mathrm{f}/2}} \tag{1}$$

where d_f is the gel fractal dimension and R_g the gyration radius of the largest fractal clusters (so that at large q the intensity decreases as q^{-d_f}, while the scattering pattern rolls off at $qR_\mathrm{g} \approx 1$).

For the entire temperature range investigated, the gel fractal dimension obtained is almost constant, with a value $d_\mathrm{f} = 1.8 \pm 0.1$, which is in reasonable agreement with the prediction for diffusion-limited cluster–cluster aggregation. Conversely, the cluster gyration radius R_g appears to show a slight monotonic decrease (from about 16 to 10 μm) on decreasing T,

although full assessment of this trend would require performing measurements at smaller q-vectors. Finally, the increase at lower temperatures of the total (integrated) scattering at small angles (which is consistent with the increase in turbidity) further confirms the progressive increase of the amount of crystallized waxes, which, ultimately, results in the formation of a macroscopically rigid gel. We note that, after a selected temperature has been reached, neither the total scattered intensity nor the scattered intensity distribution show further changes up to a timescale of a few hours. Together with the aforementioned results for α by varying the cooling rate, this suggests that, throughout cooling, the system may be considered in quasi-equilibrium as regards the total amount of precipitated waxes.

In the region between the CP and the PP, although rheological measurements show that the elastic modulus is very small, both the non-ergodic dynamics of the system and the small-angle scattering patterns are fully consistent with those of a physical gel. In order to detect the presence of a possibly exiguous residual yield stress, a preliminary investigation of gravity settling effects was carried out. Since the wax mixture and the solvent are almost buoyancy matched (density difference $\Delta\rho_0 \approx 0.015$ g cm^{-3}), the gravitational stress is expected to be very small (see below), allowing even very small values of yield stress to be probed. The restructuring of the physical gel over time followed strikingly different behaviour depending on the relative magnitude of the gravitational stress σ_g and their intrinsic yield stress σ_y. When $\sigma_y > \sigma_g$, the physical gel showed smooth compaction, at a very slow rate limited by the solvent creep flow through the structure. Conversely, when $\sigma_g > \sigma_y$, after an initial induction time, rapid collapse was found. Samples placed in test tubes 7 cm in height were first homogenized at $T = 80\,^{\circ}$C and then kept in a thermostatted bath at fixed temperature T_0. For $T_0 = 45\,^{\circ}$C, no appreciable settling was observed on a timescale of 1 day. On the other hand, a sample kept at $T_0 = 55\,^{\circ}$C showed rather fast settling, and the gel collapsed to about 70% of its initial volume in about 3 h. In addition, while the physical gel initially appeared optically homogeneous, large irregular flocks become visible at later time, suggesting a noticeable disruption of the gel structure. These observations allow us to extract a rough estimate of the gel strength. The gravitational stress gradient in the gel $\frac{d\sigma}{dz} = -\Delta\rho g\Phi$ varies with T because both the volume fraction Φ of the crystallized phase and its density difference with the surrounding fluid (which still embodies non-crystallized wax) depend on temperature. Making the very crude assumption that turbidity varies linearly with the crystallized mass, we may estimate that the volume fraction of crystallized wax is of the order of 10% at $T_0 = 45\,^{\circ}$C, but as low as $\Phi = 0.07$ at $T_0 = 55\,^{\circ}$C. With these values, the gravitation stress σ_g^{max} that the gel has to sustain at the bottom of the cell can be estimated to be of the order of $\sigma_g^{max} \approx 0.7$ Pa at $T_0 = 45\,^{\circ}$C and $\sigma_g^{max} \approx 0.04$ Pa at $T_0 = 55\,^{\circ}$C, the latter constituting a lower bound for the yield stress (in comparing these results with rheological data it should be kept in mind that gravity acts as a normal (not shear) compressive stress).

4. Conclusions

The light scattering studies reported, although carried out above the PP, provide strong support for several essential elements of the physical mechanism proposed (Visintin *et al* 2005) to account for the gelation of waxy crude oils: i.e., that attractive interactions (very probably due to dispersion forces) drive aggregation of the wax solids into an extended, fractal network. Wax precipitation progressively takes place between the CP and the PP. In this region, rapid wax aggregation leads to formation of a dynamically arrested structure, whose fractal dimension is consistent with DLCA. The strength of the network increases as the amount of crystallized wax grows, to the point that the gel becomes capable of sustaining gravitational stresses. Below the PP, the system becomes a viscoelastic solid, with a storage modulus exceeding the loss modulus.

One of the issues raised by this paper concerns the relation between dynamic arrest and mechanical rigidity. While the former requires only the build-up of a percolating network encompassing and framing all particles, the latter is related to the overall isostaticity of the structure. That is, assessment of mechanical rigidity (for a given applied stress) requires careful consideration both of the forces and of the torques acting on the structural bonds of the gel. This topic is actively investigated in simple colloidal gels, where the main control parameters are the particle volume fraction and the strength of the attractive interactions leading to gelation. A novel feature of the system investigated here is that the gel strength is strongly affected by changing the temperature. Due to the wide molecular weight distribution of the dispersed waxes, the nucleation rate strongly depends on the undercooling below CP, deep quenching leading to the formation of a much larger number of crystallites and to a large increase of the effective particle volume fraction Φ. As a consequence, the amount of undercooling tunes the competition between the rate of crystallite growth, set by the addition of single wax molecules, and that of inter-crystallite aggregation, which strongly grows with Φ. Therefore, we may expect dynamic arrest to be faster for a sample that is deeply and rapidly quenched below CP, yielding a structure characterized by small clusters made of tiny crystallites. In addition, the aggregation process becomes dependent on the thermal history of the sample. Suppose for example that the sample is conversely *slowly* quenched below CP, so that crystallites of the wax component that precipitates first are given enough time to grow and lead to system gelation. By further quenching, the additional precipitating solid phase may either grow upon the existing crystals incorporated into the already formed network, or may nucleate and grow as new crystals filling an originally tenuous structure. In both cases, we may expect the resulting structure to be different from that produced by fast quenching. Since many gelation processes of industrial interest share similar temperature effects, we believe that further studies are warranted to unravel the interplay between thermal history and resulting gel structure, which the present preliminary study can only suggest.

The rapid formation of clusters of wax solids at temperatures well above the PP revealed in the present study also provides support for an interesting hypothesis formulated recently to account for the formation of solid wax deposits onto pipe walls. These deposits can form wherever the wall temperature of the pipe through which a crude oil is flowing is lower than the CP of the oil. Though bulk gelation and deposit formation have for decades been assumed to involve fundamentally distinct mechanisms, Singh *et al* (2000) have suggested recently that wax deposition proceeds initially via the formation of a gel-like deposit. The present study suggests that there are indeed many similarities between gelation (below the PP) and deposit formation (far above the PP): wax solids formed in the oil at the pipe wall will be rapidly frozen into open aggregate structures incorporating a large volume of solvent. We can further expect these mechanically weak structures to be substantially modelled by the shear regime near the pipeline walls, as Fogler has also suggested (Singh *et al* 2000, Venkatesan *et al* 2005).

References

Chang C *et al* 1999 *J. Non-Newton. Fluid Mech.* **87** 127
Holder G A and Winkler J 1965 *J. Inst. Petroleum* **52** 228–34
Kané M *et al* 2003 *Fuel* **82** 127–35
Padgett F W *et al* 1926 *Ind. Eng. Chem.* **18** 832–5
Roberts G P *et al* 2001 *Chem. Eng. Sci.* **56** 5617–23
Rønningsen H P and Bjorndal B 1991 *Energy Fuels* **5** 895–908
Singh P *et al* 2000 *AIChE J.* **46** 1059–74
Venkatesan R *et al* 2005 *Chem. Eng. Sci.* **60** 3587–98
Visintin R *et al* 2005 *Langmuir* **21** 6240–9